Material Gain Engineering in Staggered Polar AlGaN/AlN Quantum Wells Dedicated for Deep UV Lasers

Marta Gladysiewicz, Detlef Hommel, and Robert Kudrawiec

***Abstract*—Material gain is calculated for polar staggered $Al_xGa_{1-x}N$/AlN quantum wells (QWs) of various architectures: *i)* with a step-like $Al_yGa_{1-y}N$ barrier grown prior the $Al_xGa_{1-x}N$ QW, *ii)* with a step-like barrier grown on the QW, and *iii)* with a step-like barrier grown prior and on the QW. The obtained results are compared with those obtained for reference $Al_xGa_{1-x}N$/AlN QWs. With the increase in Al concentration in the reference QW the gain peak blueshifts and its strength decreases mainly due to the Al-related increase in the electron effective mass. The step-like barrier is able to tune the spectral position of the gain peak and enhance the gain strength. For the staggered QWs with step-like barriers grown prior to the QW a blueshift of the gain peak is observed while a redshift of the gain peak is observed for QWs with the step-like barrier grown on the QW. It is shown that a strong material gain in the 260–280 nm spectral range can be achieved with the staggered $Al_xGa_{1-x}N$/AlN QW with $x = 30\%$ and 1 nm thick step-like Al_yGa1-yN barrier of high Al concentration ($y = 0.7$-0.9). The increase in Al concentration in the staggered QWs shifts the gain peak to deeper UV but the strength of material gain decreases.**

***Index Terms*—Gain, modeling.**

I. Introduction

LASERS operating in the UV-C (280–200 nm) spectral region are interesting for many applications including water purification, bio-agent detection, and pathogen sterilization [1], [2]. Among semiconductor heterostructures polar AlGaN quantum wells (QWs) are utilized as the active region for UV laser diodes (LDs) [3]–[7]. The polar LD structures are commonly fabricated on a c-plane surface orientation since it is most suitable for the growth of high-quality wurzite group-III nitrides. So far a successful realization of electrically pumped LDs with polar AlGaN QWs has been reported by a several groups [8]–[12], but despite the significant progress made in this field LDs with wavelengths shorter than 280 nm have not been reported yet. The main important challenges for realization of UV-C LDs include *i)* the reduction of large densities of defects and dislocations, *ii)* very inefficient *n*- and *p*-type conduction in Al-rich AlGaN claddings, which is associated with a high activation energy of dopants [7], and *iii)* the non-optimized active region in terms of the material gain.

The first challenge seems to be overcome, because in recent years significant progress has been made due to the development of high quality AlN substrates with low dislocation density. Currently large area AlN substrates with threading dislocation densities 3 sities of $\sim 10^3$ cm^2 are available [13]–[15]. Such substrates are natural candidates for the growth of AlGaN QWs dedicated for LDs operating in the UV-C spectral region. Moreover it has been shown that AlGaN QWs with high internal quantum efficiency ($\sim$80%) can be grown on such substrates [16], and optically pumped AlGaN QW lasers emitting in deep UV can be fabricated [17]–[20]. It means that electrically pumped AlGaN LDs operating in UV-C spectral region start to be more realistic and further progress in this field should be addressed to the carrier conduction/injection issues and the properly designed AlGaN QW region. This article is addressed to the last issue.

Due to spontaneous and piezoelectric polarization in AlGaN QWs [21], [22] the optimal QW contents and widths of the active region in LDs are very unintuitive and differ very significantly from this which is known for non-polar QWs such as InGaAs/GaAs or InGaAsP/InP QWs. In general similar material conditions are present for polar InGaN/GaN LDs. In this case very thin InGaN QWs are utilized [23]–[25] since a compromise between good quantum confinement and the large electron-hole overlap is present for 1.5–2.5 nm wide QWs. AlGaN/AlN QWs exhibit smaller built-in electric field than InGaN/GaN QWs due to weaker polarization effects. Thus conclusions from InGaN/GaN QW system (i.e., the optimal QW width etc.) cannot be completely adopted to AlGaN/AlN QWs. In addition changes in the valence band structure in AlGaN, which appear due to changes in the content of this alloy, additionally complicate the optimization of the AlGaN/AlN QW active region for LD applications.

For wurtzite structure, the top valence band at the Γ point is split into three bands due to the spin-orbit interaction and the crystal-field splitting. Because of a positive value of the

Manuscript received February 6, 2019; revised October 20, 2019; accepted October 22, 2019. Date of publication November 13, 2019; date of current version December 3, 2019. This work was supported by the National Science Centre, Poland under Grant 2013/10/E/ST3/00520. The work of R. Kudrawiec and D. Hommel was supported by the Foundation for Polish Science under Grant TEAM TECH/2016-3/16. *(Corresponding author: M. Gladysiewicz.)*

M. Gladysiewicz is with the Faculty of Fundamental Problems of Technology, Wroclaw University of Science and Technology, 50-370 Wrocław, Poland (e-mail: marta.gladysiewicz@pwr.edu.pl).

D. Hommel is with the Polish Center for Technology Development, 54-066 Wrocław, Poland (e-mail: detlef.hommel@port.org.pl).

R. Kudrawiec is with the Faculty of Fundamental Problems of Technology, Wroclaw University of Science and Technology, 50-370 Wrocław, Poland, and also with the Polish Center for Technology Development, 54-066 Wrocław, Poland (e-mail: robert.kudrawiec@pwr.edu.pl).

Color versions of one or more of the figures in this article are available online at http://ieeexplore.ieee.org.

Digital Object Identifier 10.1109/JSTQE.2019.2950802

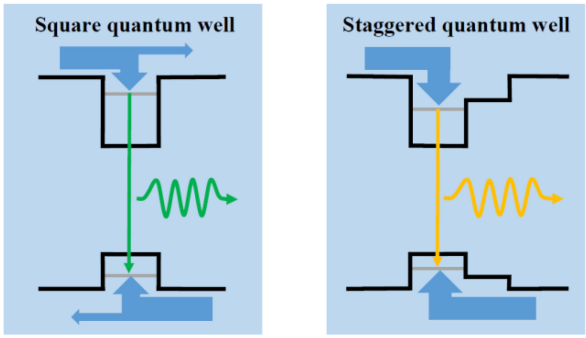

Fig. 1. Sketch of quantum confinement potential and energy levels for non-polar square QW and staggered QW.

crystal-field splitting in GaN (10 meV [26]), the topmost valence band in this compound is the heavy hole (HH) band, which is composed of atomic *p* orbitals perpendicular to c-axis. Therefore, the transition between the conduction band (CB) and HH band is allowed for electric field perpendicular to the c-axis (E⊥c). It means that the spontaneous emission is transverse-electric (TE) polarized and its propagation along the c-axis is allowed and thereby strong. Because of a negative value of the crystal-field splitting in AlN (−169 meV [26]), the topmost valence band in this compound is a crystal-field split-off (CH) band, which is composed of atomic *p* orbitals parallel to the c-axis. Therefore, the transition between the CB and CH band is allowed for electric field parallel to the c-axis (E‖c). It means that the spontaneous emission is TM polarized and its propagation along the c-axis is weak. With an increase in Al concentration in AlGaN the CH band moves closer to the CB relative to the HH band, which triggers the switch from TE- to TM-polarized emission when the CH band crosses over the HH band and thus becomes the topmost band. For AlGaN QWs grown on AlN substrate the built-in compressive strain and the quantum confinement strongly influence the light polarization for the fundamental transition.

For edge-emitting AlGaN QW LDs, it is favorable to have the active region with the fundamental transition which is TE polarized. Such conditions are rather difficult to achieve in AlN-rich AlGaN QWs and therefore LDs and light emitting diodes operating in UV-C spectral range are more challenging. To overcome this problem GaN-rich AlGaN/AlN QWs can be applied but the architecture of the QW region (i.e., compositions and thicknesses of proper layers) has to be carefully optimized in order to achieve shorter wavelengths. In this article various architectures of staggered AlGaN QWs compressively strained on AlN are carefully analyzed.

In the staggered QWs step-like barriers are introduced, see Fig. 1. In the case of non-polar QWs the influence of step-like barriers is very intuitive. Usually such barriers help to shift the emission to longer wavelengths and improve the carrier injection to the QW area as schematically shown in the sketch in Fig. 1. For polar QWs the influence of step-like barriers is less intuitive because of polarization effects that are responsible for strong electric field and thereby different shape of QW potential. In this case the staggered QWs were explored quite intensively for the InGaN material system [25], [27]–[31], but they were not intensively studied for the AlGaN material system. Only a few papers consider such a QW architecture [32], [33]. For InGaN QWs it has been shown that the step-like barrier significantly changes the confinement potential. This modyfication strongly change the electron-hole overlap and thereby influence the material gain [27]. Theoretical studies of the material gain are very important for the development of semiconductor lasers and therefore they are often performed [25], [34]–[36]. Such studies were also performed for AlGaN QWs dedicated for UV emitters [37]–[40] but the issue of staggered AlGaN QWs is still open.

II. Theoretical Approach

The electronic band structure of AlGaN QWs is calculated using 8-band ***kp*** Hamiltonian which is given in details in Ref. [37]. Because of the large band gap of AlGaN the interaction between the CB and the VB is neglected. It means that the calculation problem is reduced to the effective-mass Hamiltonian for the CB and the 6-band ***kp*** Hamiltonian for the VB. The Hamiltonian for the VB is consistent with this applied by other authors [41]–[47].

The valence band offset (VBO) between the $Al_xGa_{1-x}N$ and AlN is defined for unstrained materials, see Ref. [37]. A linear approximation is used to obtain the valence band position in AlGaN layers of different Al concentrations. In this approximation the VBO between GaN and AlN is taken from Ref. [26] to be 0.8 eV. The band gap of AlGaN is calculated using Eq. (1) with the bowing parameter $b = 0.7$ eV [26].

$$E_g^{AlGaN} = xE_g^{AlN} + (1-x)\,E_g^{GaN} - bx\,(1-x) \quad (1)$$

The influence of the compressive strain on the electronic band structure is calculated according to the Bir-Pikus model [48], details can be found in Ref. [37].

The electric field in the $Al_xGa_{1-x}N$ QW and step-like $Al_yGa_{1-y}N$ barriers is calculated according to periodic boundary conditions [49] Eq. (2)

$$F_n = \frac{\sum_q \frac{l_q P_q}{\varepsilon_q} - P_n \sum_q \frac{l_q}{\varepsilon_q}}{\varepsilon_n \sum_q \frac{l_q}{\varepsilon_q}} \quad (2)$$

where the sum runs over all the layers. ε_q, P_q, and l_q are the dielectric permittivity, total polarization, and width of the *q*-th layer, respectively. The total polarization is given by Eq. (3)

$$P_n = P_n^S + P_n^P \quad (3)$$

where P_n^S and P_n^P mean the spontaneous and piezoelectric polarization in *n*-th layer, respectively. Spontaneous polarization in $Al_xGa_{1-x}N$ alloy is calculated according to Eq. (4)

$$P_{AlGaN}^S = xP_{AlN}^S + (1-x)P_{GaN}^S + bx(1-x) \quad (4)$$

where *b* is the bowing parameter for the spontaneous polarization in $Al_xGa_{1-x}N$, which is assumed to be -0.021 C/m^2 [26]. The piezoelectric polarization was calculated using Eq. (5)

$$P_{AlGaN}^P = \left(e_{31} - e_{33}\frac{C_{13}}{C_{33}}\right)(\epsilon_{xx} + \epsilon_{yy}) \quad (5)$$

where c_{13} and c_{33} are the elastic constants, ϵ_{xx} and ϵ_{yy} are strains defined as: $\epsilon_{xx} = \epsilon_{yy} = (a_0 - a)/a$, where a_0 and a are the lattice constants of the AlN substrate and the $Al_xGa_{1-x}N$

layer, respectively. The piezoelectric tensor components (e_{31} and e_{33}), elastic constants (c_{13} and c_{33}), and remaining material parameters are calculated for AlGaN according to the linear interpolation given by Eq. (6)

$$\alpha_{AlGaN} = x\alpha_{AlN} + (1-x)\alpha_{GaN} \tag{6}$$

where α_{AlN} and α_{GaN} are parameters of binary materials. All parameters of binary semiconductors used in our calculations are taken from the review paper on material parameters in III-N [26]. For recent years some parameters were updated, but they do not vary significantly and therefore we decided to take the material parameters from one source for this study.

The material gain for AlGaN QWs is calculated for a given carrier density. This density in the CB and VB is calculated by the integration of product of the occupation probability of carriers (i.e., the Fermi-Dirac distribution) and the density of states, $\rho(k)$, over the entire band. The Fermi-Dirac distribution for electrons (f_{CB}) and holes (f_{VB}) in the QW is given by Eqs. (7) and (8)

$$f_{CB}\left(E_{CB}(k), E_{CB}^{F}\right) = \left(1+\exp\left(\frac{E_{CB}(k)-E_{CB}^{F}}{k_B T}\right)\right)^{-1} \tag{7}$$

$$f_{VB}\left(E_{CB}(k), E_{CB}^{F}\right) = \left(1+\exp\left(\frac{E_{VB}(k)-E_{VB}^{F}}{k_B T}\right)\right)^{-1} \tag{8}$$

where k_B is the Boltzmann's constant and T is temperature. Note that the carrier density determines the quasi-Fermi levels E_{CB}^{F} and E_{VB}^{F} for the CB and VB, respectively, and vice versa. The carrier density in conduction (N) and valence (P) band is calculated according to Eqs. (9) and (10)

$$N = \sum_{n_{CB}} \int_{0}^{k_{\max}} \rho(k)\, f_{CB}\left(E_{n_{CB}}(k), E_{CB}^{F}\right)\, dk \tag{9}$$

$$P = \sum_{n_{VB}} \int_{0}^{k_{\max}} \rho(k)\left[1 - f_{VB}\left(E_{n_{VB}}(k), E_{VB}^{F}\right)\right]\, dk \tag{10}$$

The integration is carried out in k space with the density of states taken from ***kp*** calculations. $k_{\max}$ is the integration limit determined by convergence of integrals given by Eqs. (9) and (10). A method based on the relaxation time approximation convoluted with a Lorentzian function ($L(n_{CB}, n_{VB}, k) = \frac{\hbar/\tau_b}{\Delta(n_{CB},n_{VB},k)^2+(\hbar/\tau_b)^2}$, where Δ is the proper energy difference) with the broadening time $\tau_b = 0.1$ ps is applied to calculate the material gain spectra [34]. In this approximation the TE and TM mode of the material gain is given by Eq. (11):

$$g_{\beta_{\mathrm{TE(TM)}}}(\hbar\omega) = C_0\beta^{-1} \sum_{n_{CB},\, n_{VB}} \int dk \left(f_{n_{CB}}(k) - f_{n_{VB}}(k)\right) \times \sum_{i,j} |M|^2_{iCB-jHH_{\mathrm{TE(TM)}}}\, L(n_{CB}, n_{VB}, k) \tag{11}$$

where $C_0 = q^2/(\omega {m_0}^2 \tau_b c \varepsilon_0)$ (q–elementary charge; ω – angular frequency, m_o – electron mass; τ_b – broadening time

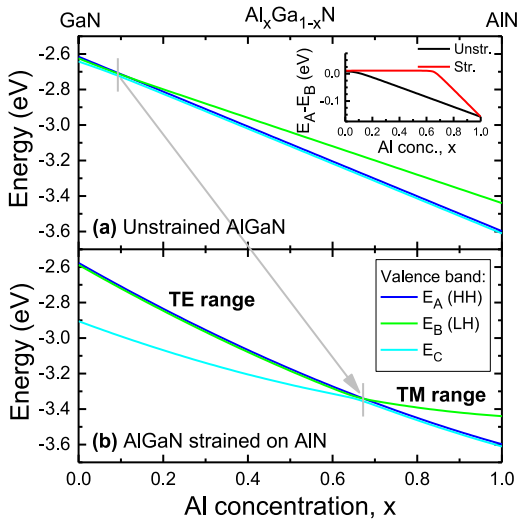

Fig. 2. Valence band position for (a) unstrained AlGaN and (b) AlGaN strained on AlN. The inset shows the energy difference between the HH and LH band.

previously defined; c – speed of light; ε_0 – dielectric constant), i and j represents, respectively, the electron and hole subbands, β in this case is the propagation constant of the TE (TM) mode, $|M|^2_{iCB-jVB_{\mathrm{TE(TM)}}}$ is the matrix element of TE (TM) mode, see details in Ref. [37].

III. Results and Discussion

Fig. 2 shows the order of valence bands in unstrained AlGaN (panel a) and AlGaN compressively strained on AlN (panel b). For unstrained AlGaN the spontaneous emission is TE polarized only for low Al concentrations since in this range the fundamental transition is between the CB and the HH band. In order to shift the QW emission to shorter wavelengths Al concentration has to be increased and therefore TE polarization of the spontaneous emission is lost. For AlGaN compressively strained on AlN (i.e., the case of AlGaN/AlN QWs) the TE polarization is preserved to much higher Al concentrations comparing to the unstrained case (~68 vs ~12%, see the grey arrow in Fig. 2) because of the strain induced modifications in the VB. The switching between the TE and the TM polarized fundamental transition is present for lower Al concentrations if AlGaN QWs are grown on virtual AlGaN substrates, see Ref. [37]. Therefore AlN substrate is the most promising choice from the viewpoint of achieving the TE polarization for light emitters in the UV-C spectral region.

According to Fig. 2(b) the strategy for obtaining an active region for light emitters with the TE polarized fundamental transition is the following: the AlGaN QW grown on AlN should be with an aluminum concentration lower that ~60% and the emission wavelength and material gain should be controlled by the QW width. Because of weak electron-hole overlaps in polar QWs only narrow QWs (1–2 nm) have a positive material gain [37]. In this case such narrow QWs can be unfavorable because of a weaker carrier injection to the active region with a deep confinement potential. It is also expected that a step-like barrier is able to improve the carrier injection. In this context

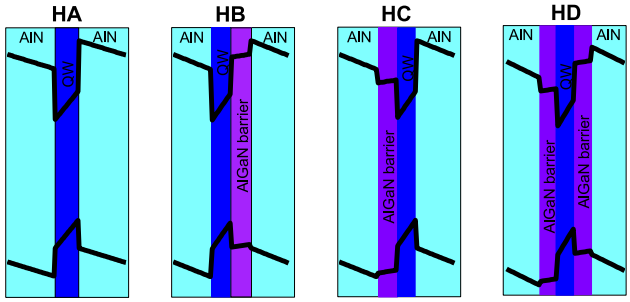

Fig. 3. Sketch of quantum confinement potential for polar QW (HA) and staggered QW with step-like barrier prior the QW (HB), on the QW (HC), and prior and on the QW (HD).

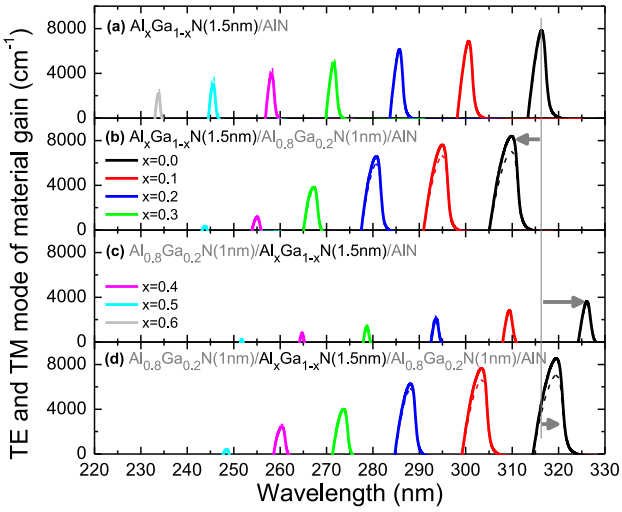

Fig. 4. TE (solid line) and TM (dashed line) mode of material gain calculated for (a) $AlxGa_{1-x}N$(1.5 nm)/AlN QW, (b) $Al_xGa_{1-x}N$(1.5 nm)/$Al_{0.8}$ $Ga_{0.2}$ N(1 nm)/AlN QW, (c) $Al_{0.8}$ $Ga_{0.2}N$(1 nm)/$AlxGa1\text{-}xN$(1.5 nm)/AlN QW, and $Al_{0.8}Ga_{0.2}N$(1 nm)/$Al_xGa_{1-x}N$(1.5 nm)/$Al_{10.8}Ga_{0.2}N$(1 nm)/AlN QW of various Al concentrations in $Al_xGa_{1-x}N$ QW. Calculations are performed for the carrier concentration of 3×10^{19} cm^{-3}.

it is interesting to calculate and analyze the material gain for staggered AlGaN QWs.

Fig. 3 shows the sketch of staggered QWs which are analyzed in this work. The heterostructure A (HA) is $Al_xGa_{1-x}N$/AlN QW which is a reference QW for staggered QWs. The heterostructure B (HB) is the staggered $Al_xGa_{1-x}N/Al_yGa_{1-y}N$/AlN QW with the step-like $Al_yGa_{1-y}N$ barrier grown prior the $Al_xGa_{1-x}N$ QW. The heterostructure C (HC) is the staggered $Al_yGa_{1-y}N/Al_xGa_{1-x}N$/AlN QW with the step-like $Al_yGa_{1-y}N$ barrier grown on the $Al_xGa_{1-x}N$ QW. In the case of non-polar QWs the HB and HC are identical from the viewpoint of the electronic band structure and the material gain, while in the case of polar QWs the two situations are completely different as will be shown in the next part of this article. It is also worth noting that the HB grown on N-polar AlN surface corresponds to the HC grown on Al-polar surface and vice versa. The heterostructure D (HD) is the staggered $Al_yGa_{1-y}N/Al_xGa_{1-x}N/Al_yGa_{1-y}N$/AlN QW with the step-like $Al_yGa_{1-y}N$ barrier grown prior and on the $Al_xGa_{1-x}N$ QW.

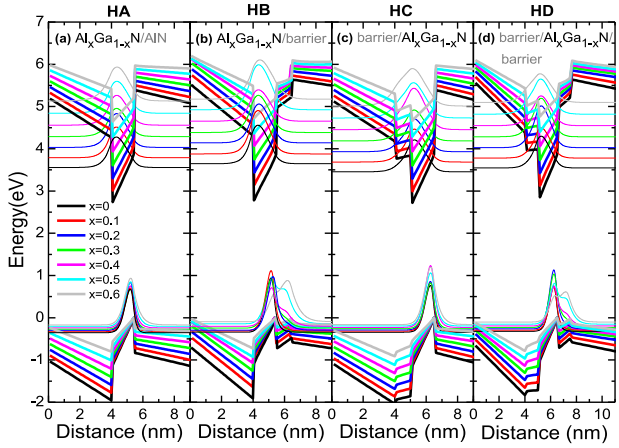

Fig. 5. Quantum confinement potentials and wavefunctions for the fundamental electron and heavy-hole state for (a) $Al_xGa_{1-x}N$(1.5 nm)/AlN QW, (b) $Al_xGa_{1-x}N$(1.5 nm)/$Al_{0.8}Ga_{0.2}N$(1 nm)/AlN QW, (c) $Al_{0.8}Ga_{0.2}N$(1 nm)/$Al_xGa_{1-x}N$(1.5 nm)/AlN QW, and $Al_{0.8}Ga_{0.2}N$(1 nm)/$Al_xGa_{1-x}N$(1.5 nm)/$Al_{0.8}Ga_{0.2}N$(1 nm)/AlN QW of various Al concentrations in $Al_xGa_{1-x}N$ QW.

Fig. 4 shows the material gain calculated for AlGaN/AlN QWs of various Al concentrations (reference heterostructures) and the staggered HB, HC, and HD. The thickness of $Al_xGa_{1-x}N$ QW and the step-like $Al_yGa_{1-y}N$ barrier is the same for all these heterostructures and equals 1.5 and 1 nm, respectively. The content of $Al_xGa_{1-x}N$ QW is changing from 0 to 60%. For $Al_xGa_{1-x}N$/AlN QWs the gain peak shifts to shorter wavelengths and its strength decreases with the increase in Al concentration, see Fig. 4(a). The blueshift of gain peak is obvious in this case and is associated with the band gap increase in AlGaN alloy. The decrease of the peak intensity may be less obvious, but having in mind that the electron-hole overlaps does not change significantly for this set of QWs, see Fig. 5(a), we can attribute this decrease in the gain maximum to the electron effective mass increase. Since the last feature is an intrinsic property of the AlGaN alloy the observed decrease of the material gain maximum at a given carrier concentration is also an intrinsic property of AlGaN/AlN QWs. The consequence of higher effective mass is the observation of a positive material gain at higher carrier concentrations for $Al_xGa_{1-x}N$/AlN QWs with higher Al content. It means that higher threshold currents are expected for lasers emitting shorter wavelengths.

To illustrate this phenomenon the material gain was calculated for different carrier concentrations for $Al_xGa_{1-x}N$/AlN QWs with x = 0, 30, and 50% Al and plotted in Fig. 6(a). In addition the threshold carrier concentration (n_{th}) was determined, see Fig. 6(b), and plotted versus the threshold wavelengths (λ_{th}) in Fig. 6(c). The threshold wavelength in this case is defined as the wavelength at which the material gain starts to be positive, see Fig. 6(a). It is worth noting that the blueshift of the gain peak with the increase in the carrier density is typical for polar QW and is associated with the partial screening of the built-in electric field and the contribution of excited states to the material gain due to their occupation at high carrier concentration [37].

It is also worth to comment that the threshold current can be strongly influenced by the material quality i.e., point defects

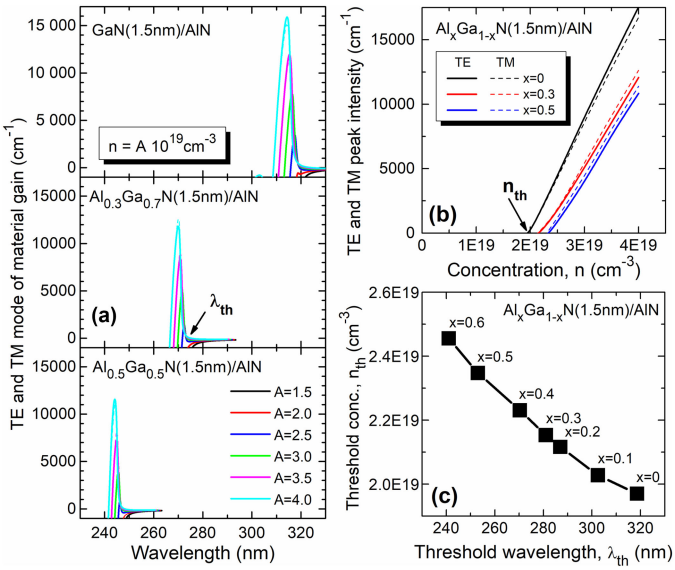

Fig. 6. (a) TE (solid line) and TM (dashed line) mode of material gain calculated for various carrier concentrations for $Al_xGa_{1-x}N$(1.5 nm)/AlN QWs with x = 0, 0.3 and 0.5. (b) The peak maximum of TE and TM mode of material gain calculated for $Al_xGa_{1-x}N$(1.5 nm)/AlN QWs with x = 0, 0.3 and 0.5.

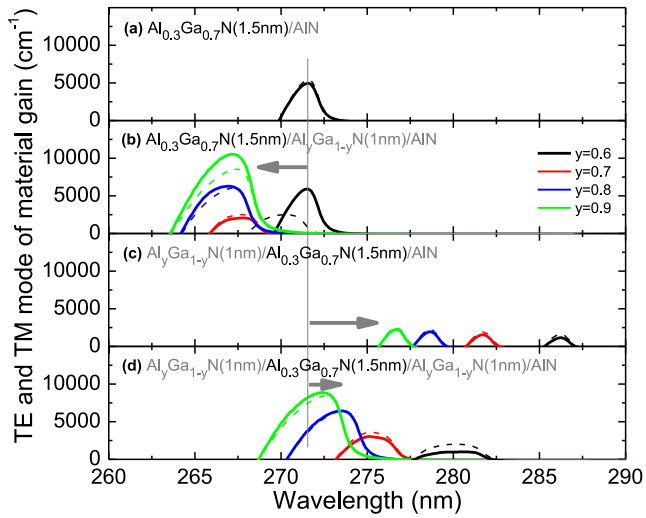

Fig. 7. TE (solid line) and TM (dashed line) mode of the material gain calculated for (a) $Al_{0.3}Ga_{0.7}N$(1.5 nm)/AlN QW and the staggered QWs: (b) $Al_{0.3}Ga_{0.7}N$(1.5 nm)/$Al_yGa_{1-y}N$(1 nm)/AlN QW, (c) $Al_yGa_{1-y}N$(1 nm)/$Al_{0.3}Ga_{0.7}N$(1.5 nm)/AlN QW, and $Al_yGa_{1-y}N$(1 nm)/$Al_{0.3}Ga_{0.7}N$(1.5 nm)/$Al_yGa_{1-y}N$(1 nm)/AlN QW of various Al concentrations in the step-like $Al_yGa_{1-y}N$ barrier. Calculations are performed for the carrier concentration of 3×10^{19} cm^{-3}.

etc. But here is a direct correlation between the threshold current and the threshold carrier concentration for a perfect QW system. Therefore the Fig. 6(c) clearly shows that an increase of threshold carrier (current) concentration is expected with a shift to shorter wavelengths.

For the staggered QWs a shift of the gain peak and a change in its strength and shape is clearly observed if we compare these QWs with the reference QWs, see curves with the same colors in Fig. 4. It is because of the polarization effects, which very strongly influence the quantum confinement potential, see Fig. 5, and thereby shift the emission wavelength and change the electron-hole overlaps. With the step-like barrier it is possible to achieve a blueshift as well as a redshift of the gain peak, see arrows in Fig. 4. Therefore the staggered polar QWs are very unintuitive regarding the expected emission wavelength and other parameters if we compare these QWs to staggered non-polar QWs.

The spectral position of the gain peak, its strength and shape also change with the thickness and content of the step-like $Al_yGa_{1-y}N$ barrier. In order to analyze this issue, $Al_xGa_{1-x}N$ QW with x = 30% has been selected since the gain peak for these QWs is in the UV-C spectral range.

Fig. 7 shows the material gain calculated for $Al_{0.3}Ga_{0.7}N$ QWs with a 1 nm thick step-like $Al_yGa_{1-y}N$ barrier of various Al concentrations. The quantum confinement potential and wavefunctions for electrons and holes for these QWs are shown in Fig. 8. It is observed that the decrease in Al concentration in step-like barriers leads to a redshift of the gain peak for all three staggered $Al_{0.3}Ga_{0.7}N$ QWs, but for the HB this shift is weaker and the gain peak position is shifted to blue if we compare it with the gain peak position for the reference $Al_{0.3}Ga_{0.7}N$/AlN QW. In addition it is clearly visible that for all these cases a decrease in the peak intensity of material gain takes place with

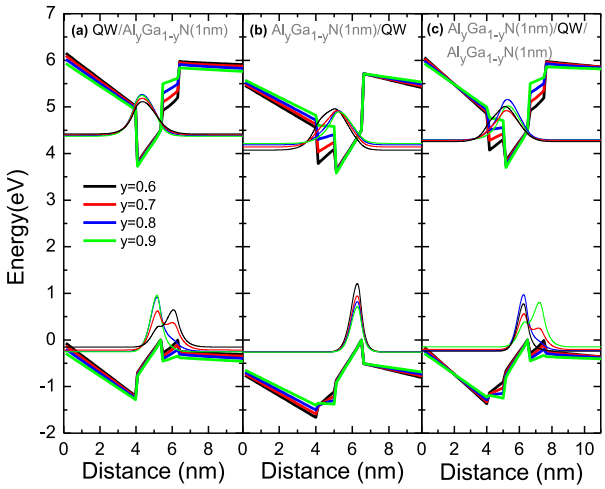

Fig. 8. Quantum confinement potentials and wavefunctions for the fundamental electron and heavy-hole state for staggered QWs: (a) $Al_{0.3}Ga_{0.7}N$(1.5 nm)/$Al_yGa_{1-y}N$(1nm)/AlN QW, (b) $Al_yGa_{1-y}N$(1nm)/$Al_{0.3}Ga_{0.7}N$(1.5nm)/AlN QW, and (c) $Al_yGa_{1-y}N$(1nm)/$Al_{0.3}Ga_{0.7}N$(1.5nm)/$Al_yGa_{1-y}N$(1nm)/AlN QW of various Al concentrations in the step-like $Al_yGa_{1-y}N$ barrier.

the decrease in Al concentration in the step-like $Al_yGa_{1-y}N$ barrier. It is because of weaker electron-hole overlap as seen in Fig. 8. Too low Al concentration in $Al_yGa_{1-y}N$ barrier allows a significant penetration of the step-like barrier by holes and electrons for HB and HC, respectively, see Fig. 8. It clearly shows that the two situations are very different. For HB it can be very unfavorable since electrons are strongly confined in the $Al_{0.3}Ga_{0.7}N$ QW while for HC it is less important since the electron wavefunction penetrates both the $Al_{0.3}Ga_{0.7}N$ QW and the step-like $Al_yGa_{1-y}N$ barrier, see Fig. 5. A very interesting situation is present for HD. In this case the bottom step-like

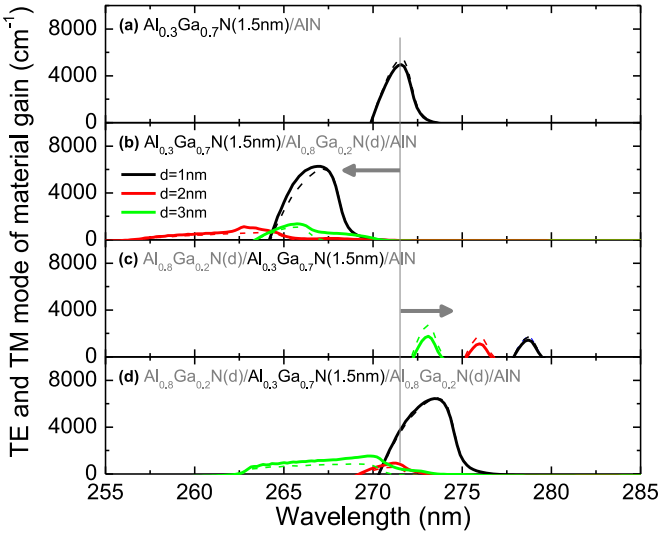

Fig. 9. TE (solid line) and TM (dashed line) mode of the material gain calculated for (a) $Al_{0.3}Ga_{0.7}N$(1.5 nm)/AlN QW and the staggered QWs: (b) $Al_{0.3}Ga_{0.7}N$(1.5 nm)/$Al_{0.3}Ga_{0.7}N$(d)/AlN QW, (c) $Al_{0.8}Ga_{0.2}N$(d)/$Al_{0.3}Ga_{0.7}N$(1.5 nm)/AlN QW, and $Al_{0.8}Ga_{0.2}N$(d)/$Al_{0.3}Ga_{0.7}N$(1.5 nm)/$Al_{0.8}Ga_{0.2}N$(d)/AlN QW of various thickness of the step-like $Al_{0.8}Ga_{0.2}N$ barrier d = 1, 2, and 3 nm. Calculations are performed for the carrier concentration of $3 \times 10^{19}cm^{-3}$.

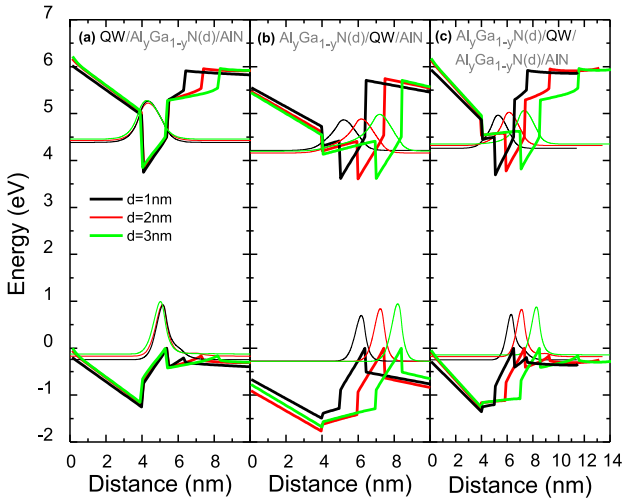

Fig. 10. Quantum confinement potentials and wavefunctions for the fundamental electron and heavy-hole state for staggered QWs: (a) $Al_{0.3}Ga_{0.7}N$(1.5 nm)/$Al_{0.3}Ga_{0.7}N$(d)/AlN QW, (b) $Al_{0.8}Ga_{0.2}N$(d)/$Al_{0.3}Ga_{0.7}N$(1.5 nm)/AlN QW, and (c) $Al_{0.8}Ga_{0.2}N$(d)/$Al_{0.3}Ga_{0.7}N$(1.5 nm)/$Al_{0.8}Ga_{0.2}N$(d)/AlN QW of various thickness of the step-like $Al_{0.8}Ga_{0.2}N$ barrier d = 1, 2, and 3 nm.

barrier leads to a penetration of this barrier by holes while the top step-like barrier leads to a penetration of this barrier by electrons. Therefore the gain peak is broader comparing to the reference QW. Comparing the gain maximum for staggered QWs and the reference QW it is observed that an enhancement of material gain is achieved for the HB and HD while HC shows significantly more weak material gain.

Similar features are observed for staggered $Al_xGa_{1-x}N$ QWs with x = 50% (not shown here). In this case we found that the Al concentration in step-like $Al_yGa_{1-y}N$ barriers cannot be too low since electrons (holes) penetrate these barriers too strongly (or even localize in these barriers if the difference between Al concentration in QW and barrier is too low). Such conditions decrease the electron-hole overlap and lead to a very broad gain spectrum compared to the reference QW and the positive material gain at higher carrier concentrations.

The analysis of the step-like barrier thickness on the gain spectrum of staggered $Al_xGa_{1-x}N$ QWs with x = 30% is shown in Fig. 9. The quantum confinement potential and wavefunctions for electrons and holes for these QWs are shown in Fig. 10. With the increase in the step-like barrier thickness the gain spectrum shifts due to changes in the quantum confinement potential. The step-like barrier is stronger penetrated by electrons with the increase in barrier thickness for the HB, see Fig. 9. Moreover a smaller energy separation between the fundamental and excited hole levels is present for the staggered HB with thicker barriers and therefore the gain spectrum is weaker and very broad in this case, see Fig. 9(b). For the HC the situation is different, the fundamental hole level is well separated from the excited hole levels and therefore the gain spectrum is narrow, see gain spectra in Fig. 9(c) and quantum confinement potentials in Fig. 10(c). A intermediate situation is observed for the HD. A strong decrease of the maximum of material gain is observed with the increase in the barrier thickness from 1 to 2 nm. Further increase in barrier thickness leads to a stronger contribution of excited hole states which is manifested by a very broad gain spectrum. From this analysis it can be concluded that the step-like barrier cannot be too thick since it leads to a localization of wavefunction in the step-like barrier. Therefore 1 nm thick step-like AlGaN barriers with high Al concentration are recommended for the staggered AlGaN QWs dedicated for UV-C LDs.

Table I summarizes the differences in material gain of HB, HC and HD in reference to the HA for structures with 30% Al in the QW region and two different Al concentration in step-like barriers (80 and 60%) at the carrier concentration equals 3×10^{19} cm^{-3}. Note to mention that these quantitative differences change with the concentration of carriers but the qualitative differences are preserved.

TABLE I
COMPARISON OF THE MATERIAL GAIN SPECTRA OF HB, HC, AND HD WITH THE REFERENCE HA AT THE CARRIER CONCENTRATION EQUALS 3×10^{19} cm^{-3}

Staggered QW structures (30 % Al in 1.5 nm wide QW and 80 % Al in 1.5 nm thick step-like barriers)	**HB**	**HC**	**HD**
TE gain maximum value, I/I_{HA}	1.26	0.39	1.30
TM gain maximum value, I/I_{HA}	1.11	0.42	1.19
Wavelength for TE gain maximum (nm)	267	279	273
Wavelength for TM gain maximum (nm)	267	279	274
Shift from the reference HA	blue	red	red

Staggered QW structures (30 % Al in 1.5 nm wide QW and 60 % Al in 1.5 nm thick step-like barriers)	**HB**	**HC**	**HD**
TE gain maximum value, I/I_{HA}	1.19	0.23	0.20
TM gain maximum value, I/I_{HA}	0.46	0.30	0.37
Wavelength for TE gain maximum (nm)	272	286	281
Wavelength for TM gain maximum (nm)	270	286	280
Shift from the reference HA	blue	red	red

Regarding the preferred light polarization of LDs, which are based on the studied QWs, it is observed that the spectral positions of TE and TM mode are almost the same for all staggered QWs as well as the reference QWs. In the analyzed range of Al concentrations it is expected since the HH and light hole (LH) band are separated by a small energy (see blue and green line in Fig. 2(b) in the range marked as the TE range). Moreover intensities of TE and TM material gain are very comparable. The TE mode is a little bit stronger than the TM mode since the HH band is the topmost valence band and thereby is stronger populated by carriers. It means that close to the threshold carrier concentration (i.e., the threshold current in electrical pumping) the TE mode will be dominating and a light with TM polarization is expected at higher carrier concentrations.

At the end of our theoretical considerations of the material gain in staggered QWs it is worth noting that the present technology allows to control the QWs width and the step-like barrier thickness with a monolayer accuracy. The molecular beam epitaxy is the recommended technique since very thin III-N QWs with sharp interfaces can be grown using this method, see for examples Refs. [50]–[52]. For the metal organic chemical vapor deposition the growth of QWs with sharp interfaces is more challenging but also possible [33].

IV. Conclusion

It has been shown that the increase in Al concentration in 1.5 nm wide $Al_xGa_{1-x}N$/AlN QWs the spectrum of the material gain blueshifts and achieves the UV-C spectral range for $x \geq 0.3$. The maximum of the material gain in these QWs decreases with the increase in Al concentration. This is mainly due to the Al-related increase in the electron (hole) effective mass. The step-like barrier in the staggered QW is able to tune the spectral position of the material gain and enhance its strength. The observed changes in the gain spectra strongly depend on the architecture of the staggered QWs as well as the content and thickness of the step-like barrier. For all three architectures, which are considered in this article (i.e., HB, HC, and HD), the thickness of step-like barrier cannot be too large since thick step-like barriers lead to electron (or hole) localization in these barriers. Therefore 1 nm thick $Al_yGa_{1-y}N$ barrier is recommended. Moreover the Al concentration in these barriers cannot be too low since it also leads to electron (or hole) localization in such barriers i.e., an unfavorable separation of wavefunctions for electrons and holes in the staggered QW. Taking into account these observations the staggered $Al_xGa_{1-x}N$/AlN QW with $x = 0.3$ and 1 nm thick step-like barrier of high Al concentration (70–90%) has been proposed for achieving the UV-C spectral range. Moreover it has been show that the situation with the step-like barrier grown prior the QW is very different from the situation with the step-like barrier grown on the QW: due to the incorporation of the step-like barrier a blueshift of the gain peak is observed for the HB while a redshift of the gain peak is observed for the HC. Such differences are not present for non-polar QWs, but they are well understood for polar QWs if we take into account polarization effects.

References

[1] T. Cutler and J. Zimmerman, "Ultraviolet irradiation and the mechanisms underlying its inactivation of infectious agents," *Anim. Health Res. Rev.*, vol. 12, pp. 15–23, 2011.

[2] H.-H. Chun, J.-Y. Kim, and K. B. Song, "Inactivation of foodborne pathogens in ready-to-eat salad using UV-C irradiation," *Food Sci. Biotechnol.*, vol. 19, pp. 547–551, 2010.

[3] A. Khan, K. Balakrishnan, and T. Katona, "Ultraviolet light-emitting diodes based on group three nitrides," *Nature Photon.*, vol. 2, pp. 77–84, 2008.

[4] H. Yoshida, M. Kuwabara, Y. Yamashita, K. Uchiyama, and H. Kan, "The current status of ultraviolet laser diodes," *Phys. Status Solidi A*, vol. 208, pp. 1586–1589, 2011.

[5] Y. Liao *et al.*, "Recent progress of efficient deep UV-LEDs by plasma assisted molecular beam epitaxy," *Phys. Status Solidi C*, vol. 9, pp. 798–801, 2012.

[6] H. Hirayama, N. Maeda, S. Fujikawa, S. Toyoda, and N. Kamata, "Recent progress and future prospects of AlGaN-based high-efficiency deep-ultraviolet light-emitting diodes," *Jpn. J. Appl. Phys.*, vol. 53, 2014, Art. no. 100209.

[7] D. B. Li, K. Jiang, X. J. Sun, and C. L. Guo, "AlGaN photonics: Recent advances in materials and ultraviolet devices," *Adv. Opt. Photon.*, vol. 10, 2018, Art. no. 43.

[8] S. Kamiyama *et al.*, "UV laser diode with 350.9-nm-lasing wavelength grown by hetero-epitaxial-lateral overgrowth technology," *IEEE J. Sel. Top. Quant. Electron.*, vol. 11, no. 5, pp. 1069–1073, Sep./Oct. 2005.

[9] H. Yoshida, Y. Yamashita, M. Kuwabara, and H. Kan, "A 342-nm ultraviolet AlGaN multiple-quantum-well laser diode," *Nature Photon.*, vol. 2, pp. 551–554, 2008.

[10] H. Yoshida, Y. Yamashita, M. Kuwabara, and H. Kan, "Demonstration of an ultraviolet 336 nm AlGaN multiple-quantum-well laser diode," *Appl. Phys. Lett.*, vol. 93, 2008, Art. no. 241106.

[11] K. H. Li, X. Liu, Q. Wang, S. Zhao, and Z. Mi, "Ultralow-threshold electrically injected AlGaN nanowire ultraviolet lasers on Si operating at low temperature," *Nature Nanotechnol.*, vol. 10, pp. 140–144, 2015.

[12] H. Taketomi *et al.*, "Over 1 W record-peak-power operation of a 338 nm AlGaN multiple-quantum-well laser diode on a GaN substrate," *Jpn. J. Appl. Phys.*, vol. 55, 2016, Art. no. 05FJ05.

[13] Z. G. Herro, D. Zhuang, R. Schlesser, and Z. Sitar, "Growth of AlN single crystalline boules," *J. Cryst. Growth*, vol. 312, 2010, Art. no. 2519.

[14] R. Dalmau, B. Moody, J. Q. Xie, R. Collazo, and Z. Sitar, "Characterization of dislocation arrays in AlN single crystals grown by PVT," *Phys. Status Solidi A*, vol. 208, pp. 1545–1547, 2011.

[15] AlN substrate products. [Online]. Available: http://www.hexatechinc.com/aln-wafer-sales.html

[16] Z. Bryan *et al.*, "High internal quantum efficiency in AlGaN multiple quantum wells grown on bulk AlN substrates," *Appl. Phys. Lett.*, vol. 106, 2015, Art. no. 142107.

[17] J. Xie *et al.*, "Lasing and longitudinal cavity modes in photo-pumped deep ultraviolet AlGaN heterostructures," *Appl. Phys. Lett.*, vol. 102, 2013, Art. no. 171102.

[18] Z. Lochner *et al.*, "Deep-ultraviolet lasing at 243 nm from photo-pumped AlGaN/AlN heterostructure on AlN substrate," *Appl. Phys. Lett.*, vol. 102, 2013, Art. no. 101110.

[19] W. Guo *et al.*, "Stimulated emission and optical gain in AlGaN heterostructures grown on bulk AlN substrates," *J. Appl. Phys.*, vol. 115, 2014, Art. no. 103108.

[20] M. Martens *et al.*, "Performance characteristics of UV-C AlGaN-Based lasers grown on sapphire and bulk AlN substrates," *IEEE Photon. Technol. Lett.*, vol. 26, no. 4, pp. 342–345, Feb.2014.

[21] F. Bernardini and V. Fiorentini, "Nonlinear macroscopic polarization in III-V nitride alloys," *Phys. Rev. B*, vol. 64, 2001, Art. no. 085207.

[22] O. Ambacher *et al.*, "Pyroelectric properties of Al(In)GaN/GaN hetero- and quantum well structures," *J Phys.: Condens. Matter*, vol. 14, 2012, Art. no. 3399.

[23] S. Nakamura, M. Senoh, N. Iwasa, and S. Nagahama, "High-brightness InGaN blue, green and yellow light-emitting diodes with quantum well structures," *Jpn. J Appl. Phys.*, vol. 34, 1995, Art. no. L797.

[24] T. Mukai, M. Yamada, and S. Nakamura, "Characteristics of InGaN-based UV/blue/green/amber/red light-emitting diodes," *Jpn. J Appl. Phys.*, vol. 38, 1999, Art. no. 3976.

[25] H. Zhao and N. Tansu, "Optical gain characteristics of staggered InGaN quantum wells lasers," *J. Appl. Phys.*, vol. 107, 2010, Art. no. 113110.

[26] I. Vurgaftman and J. R. Meyer, "Band parameters for nitrogen-containing semiconductors," *J Appl. Phys.*, vol. 94, 2003, Art. no. 3675.
[27] R. A. Arifa, Y.-K. Ee, and N. Tansu, "Polarization engineering via staggered InGaN quantum wells for radiative efficiency enhancement of light emitting diodes," *Appl. Phys. Lett.*, vol. 91, 2007, Art. no. 091110.
[28] H. Zhao *et al.*, "Growths of staggered InGaN quantum wells light-emitting diodes emitting at 520–525 nm employing graded growth-temperature profile," *Appl. Phys. Lett.*, vol. 95, 2009, Art. no. 061104.
[29] S.-H. Park, D. Ahn, and J.-W. Kim, "High-efficiency staggered 530 nm InGaN/InGaN/GaN quantum-well light-emitting diodes," *Appl. Phys. Lett.*, vol. 94, 2009, Art. no. 041109.
[30] C.-T. Liao, M.-C. Tsai, B.-T. Liou, S.-H. Yen, and Y.-K. Kuo, "Improvement in output power of a 460 nm InGaN light-emitting diode using staggered quantum well," *J. Appl. Phys.*, vol. 108, 2010, Art. no. 063107.
[31] S.-H. Park, D. Ahn, J. Park, and Y.-T. Lee, "Optical Properties of staggered InGaN/InGaN/GaN Quantum-well structures with Ga- and N-faces," *Jpn. J. Appl. Phys.*, vol. 50, 2011, Art. no. 072101.
[32] H. Lu *et al.*, "Enhancement of surface emission in deep ultraviolet AlGaN-based light emitting diodes with staggered quantum wells," *Opt. Lett.*, vol. 37, 2012, Art. no. 3693.
[33] W. Y. Wang *et al.*, "Enhancement of optical polarization degree of AlGaN quantum wells by using staggered structure," *Opt. Express*, vol. 24, 2016, Art. no. 18176.
[34] M. Gladysiewicz *et al.*, "Band structure and the optical gain of GaInNAs/GaAs quantum wells modeled within 10-band and 8-band kp model," *J Appl. Phys.*, vol. 113, 2013, Art. no. 063514.
[35] M. Gladysiewicz, R. Kudrawiec, and M. Wartak, "8-band and 14-band kp modeling of electronic band structure and material gain in Ga(In)AsBi quantum wells grown on GaAs and InP substrates," *J. Appl. Phys.*, vol. 118, 2015, Art. no. 055702.
[36] H. S. Mączko, R. Kudrawiec, and M. Gladysiewicz, "Material gain engineering in GeSn/Ge quantum wells integrated with an Si platform," *Scientific Rep.*, vol. 6, 2016, Art. no. 34082.
[37] M. Gladysiewicz, M. Rudzinski, D. Hommel, and R. Kudrawiec, "Emission and material gain spectra of polar compressive strained AlGaN quantum wells grown on virtual AlGaN substrates: Tuning emission wavelength and mixing TE and TM mode of light polarization," *Semicond. Sci. Technol.*, vol. 33, 2018, Art. no. 075003.
[38] Y. C. Yeo, T. C. Chong, M.-F. Li, and W. J. Fan, "Electronic band structures and optical gain spectra of strained wurtzite GaN–$Al_xGa_{1-x}N$ Quantum-Well lasers," *IEEE J Quant. Electron.*, vol. 34, no. 3, pp. 526–534, Mar. 1998.
[39] W. W. Chow and M. Kneissl, "Laser gain properties of AlGaN quantum wells," *J. Appl. Phys.*, vol. 98, 2005, Art. no. 114502.
[40] T. Oto, R. G. Banal, M. Funato, and Y. Kawakami, "Optical gain characteristics in Al-rich AlGaN/AlN quantum wells," *Appl. Phys. Lett.*, vol. 104, 2014, Art. no. 181102.
[41] S. L. Chuang, "Optical gain of strained wurtzite GaN quantum-well lasers," *IEEE J. Quant. Electron.*, vol. 32, no. 10, pp. 1791–1800, Oct. 1996.
[42] S. L. Chuang and C. S. Chang, "k·p method for strained wurtzite semiconductors," *Phys. Rev. B*, vol. 54, 1996, Art. no. 2491.
[43] S. L. Chuang and C. S. Chang, "A band-structure model of strained quantum-well wurtzite semiconductors," *Semicond. Sci. Technol.*, vol. 12, pp. 252–263, 1997.
[44] Y. C. Yeo, T. C. Chong, M.-F. Li, and W. J. Fan, "Electronic band structures and optical gain spectra of strained wurtzite GaN–$Al_xGa_{1-x}N$ quantum-well lasers," *IEEE J Quant. Electron.*, vol. 34, no. 3, pp. 526–534, Mar. 1998.
[45] S.-H. Park and S.-L. Chuang, "Crystal-orientation effects on the piezoelectric field and electronic properties of strained wurtzite semiconductors," *Phys. Rev. B*, vol. 59, 1999, Art. no. 4725.
[46] W. G. Scheibenzuber, U. T. Schwarz, R. G. Veprek, B. Witzigmann, and A. Hangleiter, "Calculation of optical eigenmodes and gain in semipolar and nonpolar InGaN/GaN laser diodes," *Phys. Rev. B*, vol. 80, 2009, Art. no. 115320.
[47] V. I. Litvinov, "Optical transitions and gain in group-III nitride quantum wells," *J Appl. Phys.*, vol. 88, 2000, Art. no. 5814.
[48] G. L. Bir and G. E. Pikus, "*Symmetry and Strain Effects in Semiconductors*. New York, NY, USA: Wiley, 1974.
[49] M. Leroux *et al.*, "Quantum confined Stark effect due to built-in internal polarization fields in (Al,Ga)N/GaN quantum wells," *Phys. Rev. B*, vol. 58, 1998, Art. no. R13371(R).
[50] P. K. Kandaswamy, C. Bougerol, D. Jalabert, P. Ruterana, and E. Monroy, "Strain relaxation in short-period polar GaN/AlN superlattices," *J. Appl. Phys.*, vol. 106, 2009, Art. no. 013526.
[51] P. Wolny *et al.*, "Dependence of indium content in monolayer-thick InGaN quantum wells on growth temperature in $In_xGa_{1-x}N/In_{0.02}Ga_{0.98}N$ superlattices," *J. Appl. Phys.*, vol. 124, 2018, Art. no. 065701.
[52] D. E. Sviridov *et al.*, "Direct observation of spatial distribution of carrier localization sites in ultrathin GaN/AlN quantum wells by spreading resistance microscopy," *Appl. Phys. Lett.*, vol. 114, 2019, Art. no. 061601.

Marta Gladysiewicz received the M.S. (Hons.) and Ph.D. (Hons.) degrees in physics from the Wroclaw University of Science and Technology (WUST), Wroclaw, Poland, in 1999 and 2003, respectively. Her M.S. and Ph.D. thesis were devoted to high temperature superconductors. Since 2005, her scientific activity is focused on novel semiconductor materials, including dilute nitrides, dilute bismidies, and III-Nitrides. Since 2007, she has been an Assistant Professor with the Institute of Physics, WUST. Since 2019, she has been a Professor, WUST. She was a short term Visiting Researcher with Wilfrid Laurier University, Waterloo, ON, Canada (2011 and 2014), and Lawrence Berkeley National Laboratory, Berkeley, CA, USA (2012 and 2013), where her research activity was focused on theoretical calculations of the band structure for dilute nitrides. Her current research interests include theoretical investigations of the band structure and optical properties of III–V group materials and their low-dimensional structures. Prof. Gladysiewicz was a recipient of the Student Award from the Polish Ministry of Science and Higher Education (1999). Her scientific activity was awarded by four grants from National Science Center, Poland.

Detlef Hommel received the M.S. (Hons) and Ph.D. degrees from Warsaw University, in 1975 and 1979, respectively. He has been a Professor of physics since 1994 with the University of Bremen, Germany (until 2014) and University of Wroclaw (since 2014). Educated 29 Ph.D. students. Main field of interests are optoelectronic devices of wide gap semiconductors (II–VI and group-III nitrides), semiconductor epitaxy (MBE and MOVPE) and applied physics in general. Since 2014, he has been connected with the Polish Center for Technology Development in Wroclaw (former EIT+) and Head of the Research Area "Modern Materials for Photonics and Electronics." More than 600 publications, organizer of different International Conferences (like: International II-VI Conference in 2001, International Conference on Nitride Semiconductors (ICNS) in 2005, and International Workshop on Nitrides (IWN) in 2014). Member of various International Advisory Committees. In 1996 and 2000, Visiting Professor with Yamaguchi University (Japan) and Chiba University (Japan). His current research interests include novel materials for UV emitter.

Robert Kudrawiec received the M.S. and Ph.D. (Hons.) degrees in physics from the Wrocław University of Science and Technology (WUST), Poland, in 2000 and 2004, respectively, and the D.Sc. (Habilitation) degree in physics from the Institute of Physics, WUST, in 2010. His Ph.D. thesis was devoted to dilute nitrides. During the M.S. and Ph.D. studies, he focused on applications of the modulation spectroscopy to investigate the band structure of low-dimensional systems. From 2006 to 2007, he was a Post-doctoral Scholar with Stanford University, Stanford, CA, USA, where his research was centered on the band structure and defects in GaInNAsSb–GaAs materials. From 2012 to 2013, he was a Researcher with the Lawrence National Berkeley Laboratory, Berkeley, CA, USA, where his activity was focused on novel III–V and II–VI materials dedicated for solar cell applications. Since 2018, he has been a Full Professor with the Faculty of Fundamental Problems of Technology, WUST. He has coauthored more than 300 publications in refereed journals in his research areas. Since 2017, he has been associated with the Polish Center for Technology Development at Wroclaw, where he is working on UV light emitters. His current research interests include the application of photoreflectance, contactless electroreflectance, microphotoluminescence, and time resolved photoluminescence spectroscopies to investigate the optical properties of GaN-, GaAs-, InP-, and GaSb-based materials and low-dimensional structures, and recently Van der Waals crystals.